Journal of
Ceramic Science
and Technology

Short Communication

Impact of Feedstock Nature on Thermal Conductivity of YSZ Thermal Barrier Coatings Obtained by Plasma Spraying

P. Carpio[*1, 3], M.D. Salvador[1], R. Benavente[1], M. Miranda[2], A. Borrell[1], E. Sánchez[3]

[1]Instituto de Tecnología de Materiales (ITM), Universitat Politècnica de València. Camino de Vera sn/, 46022 Valencia, Spain
[2]Centre for Advanced Structural Ceramics (CASC), Department of Materials, Imperial College London. South Kensington Campus, London SW7 2AZ, UK
[3]Instituto de Tecnología Cerámica (ITC), Universitat Jaume I. Campus Universitario Riu Sec, Av. Sos Baynat s/n, 12006 Castellón, Spain

Abstract

Yttria-stabilized zirconia (YSZ) coatings with low thermal conductivity were obtained using three different particle size distributions as starting powder: nano-, submicron- and bimodal submicron/nano-sized particles. On the one hand, these particles were reconstituted into micrometric, spray-dry agglomerates, which were subsequently deposited by means of conventional atmospheric plasma spraying (APS). On the other hand, the starting particles were dispersed in water and the resultant suspensions were deposited by means of suspension plasma spraying (SPS). The coatings were thermally treated to assess their sintering resistance. As-sprayed and thermally treated coatings were then characterized in terms of microstructure (FEG-SEM) and thermal diffusivity (laser flash equipment).

The results showed that SPS coatings exhibited extremely low thermal conductivity at low temperature which drastically augmented with increasing temperature. On the other hand, APS coatings also exhibited low thermal conductivities but their values were higher than those of the SPS coatings at the lowest temperature tested while the conductivities hardly varied with temperature.

Keywords: Thermal barrier coatings, yttria-stabilized zirconia, microstructure, thermal conductivity, atmospheric plasma spraying

I. Introduction

Thermal barrier coatings (TBCs) are essential components of gas turbine engines used in commercial aircraft and power generation. The ceramic coatings help to maintain the integrity of the underlying engine components by reducing the heat flux reached by these components [1].

The state-of-the-art material of TBCs is currently focused on yttria-stabilized zirconia (YSZ) owing to its low thermal conductivity, relativity low coefficient of thermal expansion, phase stability and high corrosion resistance [2]. The increase in the operational temperature of gas turbines results in a demand to find coatings able to present better thermal isolation [3]. Consequently, intense research activity has started in order to reduce the thermal conductivity of TBCs [4–6]. In this sense, previous research has demonstrated that using fine (nano- or submicron-sized) particles instead of coarse powder reduces the thermal conductivity of the coatings [7].

Atmospheric plasma spraying (APS) is one of the most commonly used techniques to obtain TBCs owing to its low cost and high versatility. However, particles that are too small cannot be directly injected inside the plasma plume due to their low specific weight and poor flowabil-

ity. Two possible routes can be found in the literature to overcome these constraints. The first one consists in agglomerating or reconstituting the fine particles into coarse sprayable agglomerates. Another possibility lies in the suspension plasma spraying (SPS) technique, which consists in modifying the conventional APS feeding system to inject particle suspensions instead of powders [7, 8]. Both APS and SPS techniques were addressed in this work.

The presence of unmelted or partially melted areas containing porous nano- or submicron-structured zones in YSZ coatings obtained from fine-structured powder or fine particle suspension feedstocks gives to the coating a number of valuable qualities, such as strain tolerance and low thermal conductivity as recognized in many papers in the recent literature [9]. However, despite the large number of papers in the last years dealing with the enhancement of TBCs by using nano and/or submicron-sized particles in the feedstock, few studies take into account the effect of the nature of the feedstock (powder or suspension) on the thermal properties. The relationship between the microstructure and the thermal conductivity in APS YSZ coatings has been extensively treated in the literature [4, 5]. In addition, there are also some works on the same topic in relation to the more recently researched SPS YSZ coatings [10, 11]. However, a comparison and consequently an

explanation of the differences between the thermal conductivity of APS and SPS YSZ coatings are still lacking.

The present paper focuses on the experimental comparison of thermal conductivity values of different yttria-stabilized zirconia coatings obtained from fine-structured (nano- and submicron-structured) spray-dry powders and fine particle (nano- and submicron-sized) suspension feedstocks. Microstructural changes caused by the sintering process as well as the effect of these changes on thermal conductivity are also addressed. The experiments were carried out to understand the thermal conductivity differences between YSZ APS and SPS coatings.

II. Experimental Methods

In this work, fine particle agglomerates and suspensions were deposited. In both cases, 3 mol% yttria-stabilized zirconia (YSZ) nanoparticles (5932HT, Nanostructured and Amorphous Materials Inc., USA) and submicron-sized particles (TZ-3YS, Tosoh Co., Japan) with an average particle size of 40 nm and 400 nm, respectively, a specific surface area of 25.1 and 6.8 m²/g, and tetragonal phase as the main crystalline phase were used as raw materials in both cases. Stable and well-dispersed aqueous suspensions were prepared from these particles. For this aim, a polyacrylic acid-based polyelectrolyte (PAA) was used as a dispersant and a sonication probe was utilized to break down any agglomerates. 4 % PAA and 3 min of sonication time were employed for the nanoparticle suspension, while only 0.5 % PAA and 1 min of sonication time were utilized for the submicron-sized particle suspension. A bimodal suspension was obtained by preparing nano- and submicron-sized suspensions separately, followed by mixing of the single-component suspensions with a blade-stirrer for 30 min and finally a sonication test for 1 min.

On the one hand, a reconstitution process, which consisted of spray-drying (Mobile minor, Gea Niro, Denmark) of the starting fine particle suspensions followed by a thermal treatment of the granules, was performed. The starting suspensions, with a solid loading of 30 vol%, were prepared from nanoparticles (APSn), submicron-sized particles (APSs) and a mixture of 50 % nano/submicron-sized particles (APSns) according to the procedure described above. The thermal treatments were performed at temperatures between 1000 °C and 1200 °C with a 30-min dwell time. These treatments were selected for each powder in order to reduce the porosity while avoiding a growing grain size. Then, the reconstituted powders from the starting suspensions were properly deposited by means of conventional atmospheric plasma spraying (APS). In all cases the substrate was stainless steel (AISI 304), which was grit-blasted with corundum at 4.2 bar. A bond coat (AMDRY 997, Oerlikon-Metco, Switzerland) was deposited between substrate and YSZ layer in the case of APS coatings. More details about suspension preparation, reconstitution process and APS deposition were set out in previous works [12, 13].

On the other hand, fine particle suspensions were directly deposited by suspension plasma spraying (SPS). For this aim, the APS feeding system was modified to inject liquids instead of powders into the torch. Three suspensions with a solid loading of 10 vol%, from nanoparticles (SPSn), submicron-sized particles (SPSs) and a mixture of 50 wt% nano/submicron-sized particles (SPSns) were also used for this purpose. The suspension preparation was the same as in the case of the reconstitution process. More details about SPS deposition were given in previous works [14]. The references and some specifications of the APS and SPS samples are detailed in Table 1 and the main spraying parameters are specified in Table 2.

Table 1: References and some specifications of the APS and SPS samples.

Ref.	Starting particle sizes	Feedstock	Deposition technique
APSn	100 % nanoparticles	Spray-dried powder	APS
APSns	50 % nano/ 50 % submicron-size particles		
APSs	100 % submicron-sized particles		
SPSn	100 % nanoparticles	Suspension (10 vol%)	SPS
SPSns	50 % nano/ 50 % submicron-size particles		
SPSs	100 % submicron-sized particles		

Table 2: Main spraying parameters of the APS and SPS samples.

	APS coatings		SPS coatings
	Bond coat	YSZ layer	YSZ layer
Intensity	650 A	600 A	700 A
Ar flow rate	65 slpm*	35 slpm*	37 slpm*
H_2 flow rate	8 slpm*	12 slpm*	8 slpm*
Spraying distance	145 mm	100 mm	40 mm
Spraying speed	1 m/s	1 m/s	1 m/s
Feedstock flow rate	40 g/min**	45 g/min**	27 ml/min**

* slpm: standard liter per minute
** flow rate is in mass units (g/min) in the case of APS coatings while it is in volume units (ml/min) in the case of SPS coatings.

The cross-sections of the coatings were inspected with field emission scanning electron microscopy (FEG-SEM, S-4800, Hitachi, SCSIE of the University of Valencia). For this purpose, the samples were mounted in an epoxy resin and then they were polished in a final step with 0.25 mm diamond paste. In addition, the porosity and unmelted zones were identified and quantified with image analysis (Image-Pro Plus). The coating porosity was taken into account in

order to determine the coating density. The coating density was calculated from the following expression:

$$\rho = \rho_0 \, (1-P) \qquad (1)$$

where ρ_0 is the non-porous material density (YSZ) which was estimated as 5890 kg·m^{-3},[15] and P is the coating porosity.

The thermal properties of the samples were measured using Netzsch LFA 427 – Laser Flash Apparatus, at temperatures between 25 and 1000 °C. The samples were placed in an alumina holder inside of the equipment furnace in an inert atmosphere and heated at 5 °C·min^{-1}. At least three measurements were carried out at each temperature. The lower surface of the sample was heated by means of a short energy pulse and the temperature evolution on the top surface of the sample was measured with an infrared detector. The measured values for thermal diffusivity at different temperatures with the corresponding specific heat and density of the samples were used to calculate the thermal conductivity by means of the *Proteus*®Software of the equipment using the following equation:

$$\lambda(T)=C_P(T) \, \rho \cdot a(T) \qquad (2)$$

where λ is the thermal conductivity (W·m^{-1}·K^{-1}), $C_P(T)$ is the specific heat (J·kg^{-1}·K^{-1}), ρ is the coating density (kg·m^{-3}) and a is the thermal diffusivity (m^2·s^{-1})[16].

For the thermal characterization of the multilayer coating sample (metallic substrate plus bond and top layers), it was first necessary to perform an initial thermal characterization of the steel substrate using the "Cowan+pulse correction" diffusivity model for the processing of the data. The thermal properties of the different zirconia coatings were measured directly with the substrate using a bilayer model for the calculation of thermal diffusivity in the coating layer and the specific heat provided in ref.[16]. For each coating composition, at least two specimens were tested. The tested specimens were disks with diameters of ~12.5 mm.

The changes in the microstructure caused by the sintering effect were also evaluated. For this goal, the samples were isothermally treated at 500 °C for 1 h. Then porosity and unmelted areas were quantified before and after the isothermal treatment and the microstructural changes were related to the evolution of the thermal conductivity.

III. Results and Discussion

Microstructural features of YSZ coatings obtained from fine-structured powders (nano- or submicron-structured) or fine particle suspensions (nano- or submicron-sized) have been extensively reported elsewhere[9–12]. Overall these coatings display common features which consist of a two zone-type (bimodal) microstructure, as can be observed in the as-sprayed coatings of Fig. 1a (APS coating) and Fig. 2a (SPS coating). It should be noted that in these figures, micrographs of SPS samples were taken at higher magnifications due to their thinner thickness (220 µm approximately in APS coatings versus 30 µm in SPS coatings). Thus this bimodal microstructure which typically occurs when feedstocks of fine-structured spray dry powders or fine particle suspensions are used comprises unmelted zones (marked U) surrounded by a melted matrix

(marked M)[9]. The values of porosity and unmelted areas determined by images analysis are plotted in Fig. 3. In spite of the similarities between APS and SPS microstructures, substantial differences attributed to the nature of the feedstock (powder or suspension) also exist. Hence in the case of APS coatings, unmelted zones are well identified throughout the coating because they were the consequence of partially melting of the fine-structured spray-dry agglomerates[8]. Even in some cases the nano- or submicron-structure of these agglomerates is almost fully preserved inside the coating. On the other hand, although SPS process involves stabilized particle suspensions when these suspensions are fed into the plasma torch they undergo undesirable agglomeration due to a sudden solid concentration increase associated with the flash evaporation of water. In addition, much more plasma enthalpy is necessary to evaporate the water in SPS deposition, consequently the amount of unmelted zones strongly increases in comparison with APS process[7]. With regard to porosity, no significant differences were observed between both types of coatings while the values calculated were consistent with the typical values reported in the literature for APS and SPS YSZ coatings[5,11]. It is important to take into account that SPS coatings exhibit very little pores due to their reduction of the splat size. Therefore, small pores can hardly be identified by image analysis and the porosity of SPS samples is probably higher than the values displayed in Fig. 3[17]. Nevertheless, these little pores are beneficial for the thermal conductivity reduction, as explained below[10].
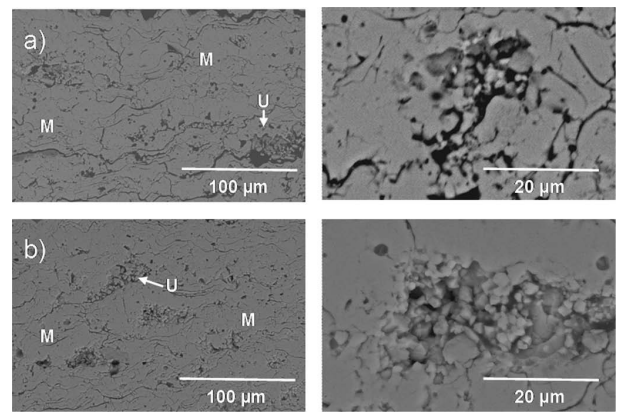

Fig. 1: FEG-SEM micrograph of APS coating (APSn) at different magnifications: a) as-sprayed coating; b) coating treated at 500 °C.
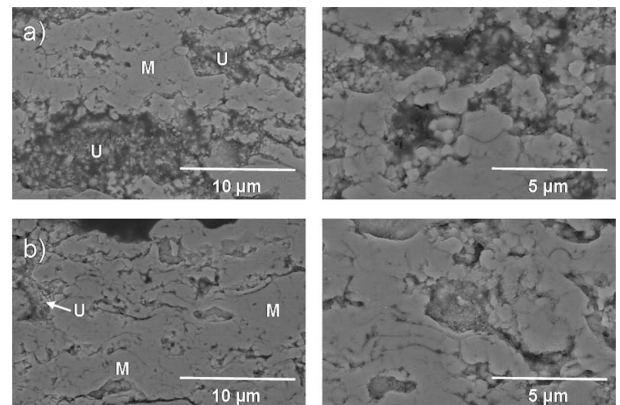

Fig. 2: FEG-SEM micrograph of SPS coating (SPSn) at different magnifications: a) as-sprayed coating; b) coating treated at 500 °C.
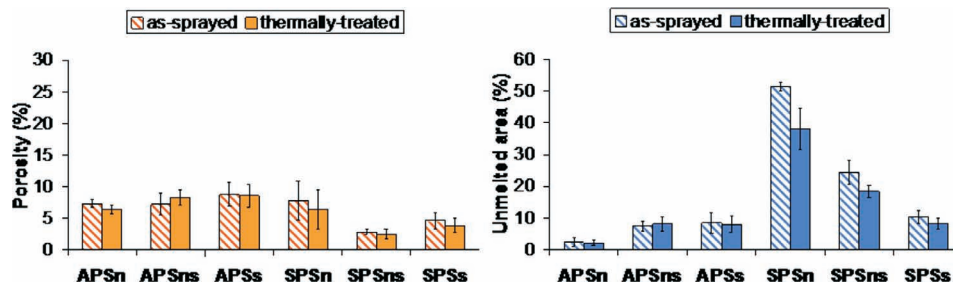
Fig. 3: Porosity and unmelted area of the as-sprayed and thermally treated coatings.

Among the coatings deposited with the same technique (APS or SPS), the effect of the particle size (nano, submicron or nano/submicron) in the feedstock on the amount of unmelted regions showed differences. Thus SPSn coating (100 % nanoparticle feedstock) contains a large amount of unmelted area (approx. 50 %) as a consequence of the high trend to agglomeration of nanoparticles when the water is removed. In this sense when submicron-sized particles form part of the feedstock the amount of these unmelted regions is strongly reduced due to a decreasing agglomeration process of these coarser particles in comparison with nanoparticles. As observed the coating obtained from feedstock SPSns (50 % nano-/50 % submicron-sized particles) shows intermediate behavior between SPSn and SPSs coatings. With regard to APS coatings, they contain much fewer unmelted areas than SPS coatings as explained above. Nevertheless, the amount of unmelted areas follow the opposite variation since these areas grow as the amount of submicron-sized particles in the feedstock augments. This is because nanoparticles enhance the sinterability of the fine-structured spray-dried agglomerates of the APS feedstocks.

Thermal conductivity of the coatings at different temperatures is plotted in Fig. 4. As it can be observed APS coatings show quite low thermal conductivity as consequence of the increase of grain boundary contribution to phonon scattering associated with the nano- or submicron-sized structure of the coating [18]. These findings agree with those reported in the literature [4,5] for these types of fine-structured coatings. Bearing in mind this argument when the amount of nanoparticles in the feedstock grows (from APSs to APSn samples) thermal conductivity should in principle decrease due to the nanostructured nature of the aforementioned partially melted zones. Nevertheless, this decrease in thermal conductivity is to some extent compensated by the reduction of the amount of unmelted areas in the coating occurring when the feedstock contains more nanoparticles as set out above. More interestingly at low temperature (50 °C) any of the SPS coatings display extremely low thermal conductivities (0.08 – 0.35 W·m^{-1}·K^{-1}), which are much lower than those of any of the APS coatings. This reduced thermal conductivity in SPS samples is caused by the high amount of nano- or submicron-sized porosity retained in the many unmelted zones present in these coatings as set out above [10]. Unfortunately, such low porosity cannot be measured by means of standard imaging analysis techniques [7,17]. It is worth mentioning that despite the higher value of thermal

conductivity of the SPSs coating (100 % submicron-sized particles), no significant differences in thermal conductivity at low temperature were found among the three SPS coatings. These findings highlight the role of the melted matrix fine-structure (pores, different type of cracks…) of SPS coatings on the thermal conductivity [10]. Further research is still necessary to clarify the contribution of this melted matrix to thermal conductivity.
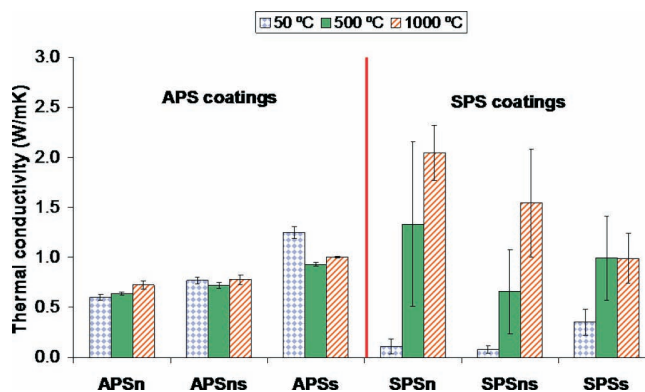

Fig. 4: Thermal conductivity at different temperatures of the coatings.

Apart from the differences observed between the thermal conductivity of APS and SPS coatings at low temperature the evolution of thermal conductivity with temperature also displayed significant differences between both types of coatings (APS and SPS series). Thus, SPS coatings exhibit a stronger thermal conductivity variation (increasing) with temperature in comparison with APS coatings, which showed quite robust behavior with scarce variation with temperature. In fact, the thermal conductivity increase in APS coatings was only observable with the coating obtained from APSn feedstock, i.e. the feedstock formed exclusively by nanoparticles, due to the higher tendency to sintering of the preserved, unmelted nanoparticle zones [12]. Although, the APSs (from submicron-sized particles feedstock) coating showed an opposite effect (decrease in thermal conductivity with temperature), this variation was probably to do with an unexpected high thermal conductivity of the low-temperature coating as compared with the other two coatings at the same temperature (APSn and APSns).

As the thermal conductivity of bulk sintered YSZ is reduced with increasing temperature due to phonon conduction effect as reported elsewhere [2], thermal conductivity evolution of APS and SPS coatings should be ex-

plained by microstructural changes occurring when the temperature increases. In order to explain these thermal conductivity variations, APS and SPS coatings were thermally treated at 500 °C for 60 min as set out above. The sintered coating microstructures are shown in Fig. 1.b and Fig. 2.b whereas porosity and unmelted area values are shown in Fig. 3. Comparing microstructures between as-sprayed and thermally-treated coatings, it can be observed that the sintering effect was much higher in SPS coatings, probably because unmelted zones were less porous and above all because this porosity was made up of very small (nanoscale) pores as reported elsewhere [7]. Therefore, as expected the SPSn (100 % nanoparticle feedstock) coating is affected by sintering the most, while with the addition of submicron-sized particles to the feedstock manage, the sintering effect could be moderated. The sintering effect is revealed as a reduction of porosity while the coating thickness is almost invariable.

In the case of APS coatings, sintering effect was almost negligible. In fact, the porosity increases slightly with sintering temperature in the case of APSns coating although this finding could be associated with the unmeasurable size of pores as set out above. In this sense in previous work it was demonstrated that APS coatings from nanostructured powders could exhibit improved sintering resistance compared with their conventional counterparts (obtained from microstructured powders) because nanostructured unmelted zones act as porosity former regions during thermal treatment [18]. Nevertheless, this effect cannot be observed in SPS coatings since their nano- or submicron-structured unmelted zones sinter too fast.

IV. Conclusions

YSZ coatings were obtained with APS and SPS techniques from three different particle size distributions as starting powder (100 % nanoparticles, 100 % submicron-sized particles and 50 %/50 % nano- and submicron-sized particles).

In the case of SPS coatings, extremely low thermal conductivities values were obtained at room temperature as a consequence of the nano or submicron features of both the particles and pores that made up of the coating structure, in particular those pores and particles comprising the unmelted regions of the coating. However, sintering resistance of these coatings was also low, therefore thermal treatment after deposition results in significant structural changes that negatively affect the thermal conductivity (thermal conductivity increase) at high temperature. The higher the nanoparticle content in the feedstock the stronger the thermal conductivity increases with temperature in the resulting SPS coating is.

On the other hand, APS coatings also display low thermal conductivity at room temperature, which is higher than that of the SPS coatings as a consequence of the fewer unmelted areas in APS coatings when compared with SPS coatings. On the contrary, APS coatings exhibit quite a robust behavior since their thermal conductivity hardly varies with increasing temperature owing to the lower sintering trend of their constituent unmelted zones.

Acknowledgments

References

[1] Padture, N.P., Gell, M., Jordan, E.H.: Thermal barrier coatings for gas-turbine engine applications, *Science*, **296**, 280 – 284, (2002).

[2] Tian, Y.S., Chen, C.Z., Wang, D.Y., Ji, Q.: Recent developments in zirconia thermal barrier coatings, *Surf. Rev. Lett.*, **12**, 369 – 378, (2005).

[3] Curry, N., Markocsan, N., Li, X.H., Tricoire, A., Dorfman, M.: Next generation thermal barrier coatings for the gas turbine industry, *J. Therm. Spray Techn.*, **11**, 108 – 115, (2011).

[4] Wang, Y., Wu, W., Zheng, X., Zeng, Y., Ding, M., Zhan, C.: Relationship between the microstructure and thermal conductivity of plasma-sprayed ZrO_2 coatings, *J. Therm. Spray Techn.*, **20**, 1177 – 1182, (2011).

[5] Tan, Y., Sriniwasan, V., Nakamura, T., Sampath, S., Bertrand, P., Bertrand, G.: Optimizing compliance and thermal conductivity of plasma sprayed thermal barrier coatings via controlled powders and processing strategies, *J. Therm. Spray Techn.*, **21**, 950 – 962, (2012).

[6] Pawłowski, P., Fauchais, P.: Thermal transport properties of thermally sprayed coatings, *Int. Mater. Rev.*, **37**, 271 – 289, (1992).

[7] Fauchais, P., Montavon, G., Lima, R.S., Marple, B.R..: Engineering a new class of thermal spray nano-based microstructures from agglomerated nanostructured particles, suspensions and solutions: an invited review, *J. Phys. D Appl. Phys.*, **44**, 093001, (2011).

[8] Pawłowski, L.: Finely grained nanometric and submicrometric coatings by thermal spraying: A review, *Surf. Coat. Technol.*, **202**, 4318 – 4328, (2008).

[9] Lima, R.S., Marple, B.R.: Thermal spray coatings engineered from nanostructured ceramic agglomerated powders for structural, thermal barrier and biomedical applications: A review, *J. Therm. Spray Techn.*, **16**, 40 – 63, (2007).

[10] Carpio, P., Blochet, Q., Pateyron, B., Pawłowski, L., Salvador, M.D., Borrell, A., Sánchez, E.: Correlation of thermal conductivity of suspension plasma sprayed yttria stabilized zirconia coatings with some microstructural effects, *Mater. Lett.*, **107**, 370 – 373, (2013).

[11] VanEvery, K., Krane, J.M., Trice, R.W., Wang, H., Porter, W., Besser, M.: Column formation in suspension plasma-sprayed coatings and resultant thermal properties, *J. Therm. Spray Techn.*, **20**, 817 – 28, (2011).

[12] Carpio, P., Moreno, R., Gómez, A., Salvador, M.D., Sánchez, E.: Role of suspension preparation in the spray drying process to obtain nano/submicrostructured YSZ powders for atmospheric plasma spraying, *J. Eur. Ceram. Soc.*, **35**, 237 – 247, (2015).

13 Vicent, M., Sánchez, E., Moreno, A., Moreno, R.: Preparation of high solids content nano-titania suspensions to obtain spray-dried nanostructured powders for atmospheric plasma spraying, *J. Eur. Ceram. Soc.*, **32**, 185 – 194, (2012).

14 Carpio, P., Bannier, E., Salvador, M.D., Borrell, A., Moreno, R., Sánchez, E.: Effect of particle size distribution of suspension feedstock on the microstructure and mechanical properties of suspension plasma spraying YSZ coatings, *Surf. Coat. Technol.*, **268**, 293 – 297, (2015).

15 Lide, D.R.: CRC handbook of chemistry and physics. CRC, Boca Raton, 2008.

16 West Conshohocken, P.A.: Standard test method for thermal diffusivity by the flash method. ASTM Standard E1461 – 11, (2012).

17 Bacciochini, A., Montavon, G., Ilavsky, J., Denoirjean, A., Fauchais, P.: Porous architecture of SPS thick YSZ coatings structured at the nanometer scale (~50 nm), *J. Therm. Spray Techn.,* **19**, 198 – 206, (2010).

18 Lima, R.S., Marple, B.R., Nanostructured YSZ thermal barrier coatings engineered to counteract sintering effects, *Mater. Sci. Eng. A*, **485**, 182 – 193, (2007).